Research Article

Multi-Response Optimization and Cell Structure-Property Relationships of Polylactide (PLA) Foams

Yusuf Arya Yudanto*
School of Integrated Science and Innovation, Sirindhorn International Institute of Technology (SIIT), Thammasat University, Pathum Thani, Thailand

Atitsa Petchsuk
National Metal and Materials Technology Center (MTEC), National Science and Technology Development Agency (NSTDA), Thailand Science Park, Pathum Thani, Thailand

Pakorn Opaprakasit*
School of Integrated Science and Innovation, Sirindhorn International Institute of Technology (SIIT), Thammasat University, Pathum Thani, Thailand

* Corresponding author. E-mail: yusuf.ary@dome.tu.ac.th, pakorn@siit.tu.ac.th DOI: 10.14416/j.asep.2024.06.011
Received: 28 December 2023; Revised: 19 February 2024; Accepted: 29 March 2024; Published online: 27 June 2024

Abstract
The renewability and ease of processing of polylactide (PLA) make it ideal for disposable foam products. However, controlling the foam structure is challenging due to its low melt strength and crystallization ability, which can result in cell rupture-prone and excessively large cells, necessitating a comprehensive understanding of the influences of foaming parameters (temperature, pressure, and time) on cell structures and properties to unlock PLA's full potential. This study optimizes the fabrication of PLA foams using solid-state batch foaming under supercritical CO_2 conditions by employing a central composite design of response surface methodology. Single-parameter investigations reveal that higher foaming temperature, increased pressure, and longer foaming time increase the apparent density due to reduced polymer viscosity, pressure-dependent gas entrapment, and enhanced gas diffusion, leading to faster cell nucleation and cell formation. The compressive properties depend on stress-strain behavior and cell morphology, influenced by the cell shape and wall thickness. Thicker cell walls delay cell buckling and improve compression resistance. Higher sphericality evenly distributes compressive stress across cell surfaces, enhancing the foam's resilience against localized collapse. Multi-response optimization successfully fabricated lightweight PLA foam (0.134 g/cc apparent density) with enhanced compressive modulus (1.955 MPa at 50% strain) and controlled cell morphology (average cell size of 21.055 μm and cell density of 52.385×10^5 cells/cm^3) at optimized foaming conditions (180 °C, 165 bar, and 2.3 h). The PLA foams have potential as a reusable and degradable absorbent for liquids and oils, but there are challenges in scaling production.

Keywords: Cell morphology, Compressive behavior, PLA foam, Response surface methodology, Supercritical CO_2

1 Introduction

Plastics' affordability, versatility, and high durability in diverse forms (solids, liquids, solution, latex, or suspension) have fueled their widespread use, with polymeric foams being a particularly popular product [1]–[4]. Polymeric foam, typically produced by saturating a polymer with a gas (physical or chemical)

to achieve a desired cellular structure (open-cell or closed-cell) with specific thermal, mechanical, or acoustic properties, gains its cellular structure [5], [6]. These cellular structures can be smaller than 30 μm with cell densities ranging from 10^9 to 10^{12} cells/cm^3, making them microcellular foam [6], [7]. Notably, these foams possess remarkable properties, often surpassing their solid counterparts, offering excellent mechanical performance, economical production, and low material volume. These have found applications in various fields, *e.g.*, packaging and cushioning [8], [9], insulation [10], [11], liquid absorption and filtration [12], flame retardant [13], building and construction [7], [14], [15], sports equipment [16], and biomedical field [17], [18].

Polylactide (PLA) is emerging as a promising candidate for sustainable alternatives to environmental concerns over fossil-based polymers due to its renewability, sustainability, biocompatibility, degradability, and processability [19], [20]. PLA is widely employed as nanoparticles for cosmetic applications [21]–[23], drug encapsulation templates in biomedical fields [24], toughening agents [25]–[28], nanofibers for oil absorption and oil/water separation [29], [30], and bio-composites for packaging [23], [31]. These mentioned renowned enable its foam counterparts to be utilized as disposable meal boxes or reefer containers for food packaging and fresh-keeping [32], [33]. The potential for further diverse applications is contingent upon these foams' apparent density and cell morphology [34]. In this context, the use of supercritical carbon dioxide (sc-CO_2) as a physical blowing agent for PLA foaming has gained vast attention due to its high polymer solubility, eco-friendliness, high efficiency, non-toxicity, and moderate critical conditions [35]–[38]. However, the fabrication and applications of PLA foam are constrained by its low melt strength and crystallization ability, rendering it susceptible to cell rupture and producing excessive cell sizes [39], [40]. Previous studies have focused on optimizing the foaming process to control cell morphology [40]–[42]. Mahdavi *et al*. [43] prepared PLA foams by optimizing the foaming parameters by injecting a physical blowing agent into a high-pressure vessel, resulting in a more homogeneous cell structure at 90 bar and 70 °C. Increasing pressure caused a decrease in cell size and an increase in cell density, impacting the foams' compressive modulus and compressive strength [7]. Various variables, including temperature, pressure, and time, influence the final properties of PLA foams, emphasizing the importance of understanding the relationship between the foaming conditions and the cellular morphology to improve the foamability of this degradable polymer [44], [45].

The current study simultaneously investigates cell morphology and its effect on other properties, including apparent density and compressive modulus of PLA foams fabricated *via* solid-state batch foaming with supercritical CO_2 as a physical blowing agent. Central composite design (CCD) is used as the baseline for the design of experiment (DoE) through a combination of response surface methodology (RSM) to determine the most influential foaming process parameter. Multi-objective optimization is then used to determine the optimal foaming process conditions based on the desirability profile, thereby verifying the CCD-RSM-built model.

2 Materials and Methods

2.1 *Materials*

Pelletized PLA (Ingeo™ 4043D), with a melting temperature of 153 °C, specific gravity of 1.24 g/cc, and glass transition temperature (T_g) of 58 °C, was dried at 80 °C for 4 h to reduce the moisture content to 0.025% to prevent hydrolysis during the process. Carbon dioxide gas (99.8% purity) was used as a blowing agent.

2.2 *Preparation and characterization of PLA foams*

PLA foams were prepared using a batch foaming process assisted by sc-CO_2. Dried PLA pellets were weighed, loaded into a foaming vessel, and melted at 180 °C for 30 min. The CO_2 gas was then introduced into the vessel at controlled pressure and temperature according to the experimental design. Finally, the temperature was lowered to 80 °C, and the gas was slowly released (depressurization) to induce cell nucleation and growth. The foam structures were formed after the autoclave was cooled to ambient temperature. The process steps are summarized in Figures 1 and 2. This study employed a supercritical fluids apparatus developed by MTEC, comprising a pressurized vessel with a heater and connected *via* steel

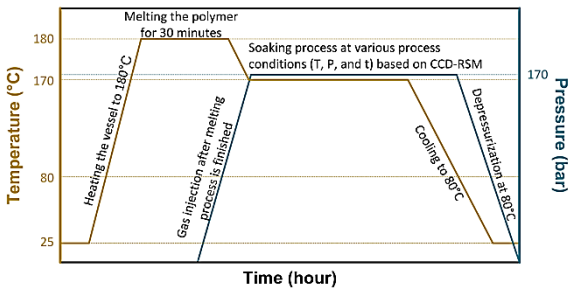

Figure 1: The overall foaming procedure of PLA.

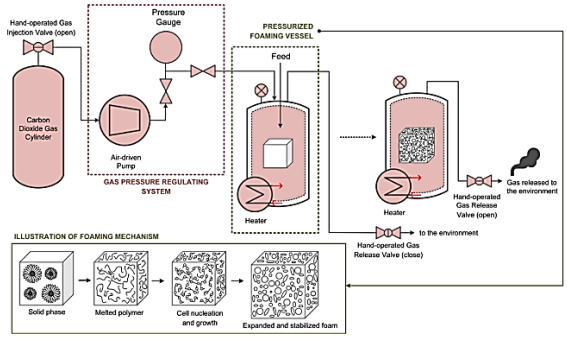

Figure 2: The schematic diagram for the foaming mechanism of PLA.

pipes to a CO_2 gas tank for injection. The apparatus is equipped with valves for pressure regulation and gauges for monitoring pressure and temperature, and it employs precise temperature control mechanisms.

The foamed samples were freeze-fractured, gold-sputtered, and examined using a scanning electron microscope (FE-SEM SU5000, Hitachi, Japan) at 5 kV to asses their cellular structure and morphology. The NIS Elements software was used to quantitatively assess the number of cells (n) in a specific area, where at least 200 cells were analyzed. The total number of cells in each micrograph, area (A), was then determined. The cell density (N_0) was calculated using Equation (1) below [14], [46].

$$N_0 = \left(\frac{n \times M^2}{A} \right)^{3/2} \times FR \quad (1)$$

where n represents the cell number in a certain area A in cm^2 by operating on the assumption that the cellular structures are spherical and distributed uniformly, M is the magnification factor, and FR is the foaming ratio, calculated using Equation (2) below [47].

$$FR = \frac{\rho_p}{\rho_f} \quad (2)$$

where ρ_p is the density of polymer in pellet form, and ρ_f is the foam density.

Equation (3) was then utilized to determine the cell size (N_s) of the foam [14].

$$N_s = \left(\frac{FR - 1}{N_0} \right)^{1/3} \quad (3)$$

where N_s is the cell size in μm, and N_0 is cell density in cells/cm^3.

The apparent density (ρ_f) of the foam was calculated using the displacement method, as described in ASTM D792 [48], utilizing a density kit (Density Kit Standard & Advanced, Mettler Toledo, Switzerland) installed in a digital balance.

Compressive testing of the foams was performed following ASTM D695 [49] using a universal testing machine (H5KT, Tinius Olsen, United Kingdom) at room temperature. Standard-sized specimens (12.7 mm in diameter and 25.4 mm in length) were tested at a crosshead speed of 0.8 mm/min and a target force of 4500 N.

The foams with the highest foaming ratio were selected for absorption analysis. Dried samples (10 mm in diameter and thickness) were immersed in various test liquids (DI water, ethyl acetate, cyclohexane, silicone oil, soybean oil, and motor oil) at room temperature according to ASTM D570 [50]. The test specimens were carefully cut to produce a smooth and crack-free edge. After immersion at regular intervals (10, 30, 60, 90, and 120 min), the foams were removed, drained for 30 s [51], and weighed to determine the absorption capacity using the following Equation (4).

$$Absorption\,capacity\ (g/g) = \frac{W_t - W_0}{W_0} \quad (4)$$

where W_0 is the initial weight (dry sample) and W_t is the final weight (wet sample).

The foams' reusability was evaluated to assess their long-term absorption performance. A modified version of the procedure reported by Xiao *et al*. [52] was employed. After each 120 min immersion cycle, the foams were soaked in ethanol to remove the test liquids and dried at 60 °C until their weight was stabilized. This test was repeated for n cycles.

2.3 *Experimental design and mathematical modeling*

The Design-Expert 13 software was used to create an experimental design using the central composite design of response surface methodology (CCD-RSM), summarized in Table 1. This design was used to study the effect of process parameters on the properties of PLA foams, *i.e.*, cell morphology, apparent density, and compressive modulus. The three most important process parameters (foaming temperature, pressure, and time) were divided into five levels for this study: one center level, two factorial levels, and two-star levels determined orthogonally. The Design-Expert 13 software was also used for data analysis, visualization, statistical analysis (ANOVA), quadratic model construction, and perturbation analysis to investigate the effects of foaming temperature, pressure, and time on the responses using three-dimensional response surface plots.

Table 1: Summary of the factors and levels used for CCD-RSM

Factors	Symbol	Coded Factor Levels				
		$-\alpha$	–1	0	+1	$+\alpha$
Foaming Temperature (°C)	A	144.26	150	170	190	195.74
Foaming Pressure (bar)	B	144.26	150	170	190	195.74
Foaming Time (h)	C	1.28	1.5	2.25	3	3.22

3 Results and Discussion

3.1 *Cell Morphology and size distribution tests*

A broad outline of the foam's cell morphology is crucial as it significantly impacts the foamability of polymers and their physical and mechanical properties, such as density and compressive strength [53], [54]. The cell structures and morphology in the resulting PLA foams are affected by the foaming temperature, as depicted in Figure 3. A foaming pressure of 170 bar and a time of 2.25 h were used for these particular samples. Foaming at 144.26 and 195.74 °C results in a homogeneous cell structure with completely closed cell walls. Conversely, foams produced at 170 °C display non-uniform cell distribution, with sizes spreading from big to extremely small. This irregularity is attributed to the low melt strength of PLA, particularly at 195.74 °C, leading to cell wall rupture and larger cell sizes. The size distribution of all samples follows a Gaussian distribution, which provides a useful approximation of the cell size distribution, presuming that the cells are spherical and the process of cell nucleation and growth is random [55], [56]. The cell size decreases at higher temperatures of 170 °C due to increased CO_2 solubility in the polymer melt, leading to smaller cells. Sundarram *et al*. [17] observed a decrease in cell size with increasing temperature, from 203–117 μm, due to enhanced nucleation and limited cell growth. At the highest foaming temperature of 195.74 °C, cell size increases due to the reduced polymer stability (too porous) and enhanced chain mobility, leading to cell wall rupture and coalescence [57], [58]. The cell sizes of 20.2 μm (low temperature), 15.1 μm (mid temperature), and 20.7 μm (high temperature) were observed in this study, reflecting that the foams produced under the conditions described in Figure 3 are microcellular [6], [7].

The cell morphology of PLA foams prepared at various foaming pressures is compared in Figure 4. A flower-like cell structure was observed in the samples foamed at 144.26 bar, as outlined with a red circle. Also, the cell walls appeared to be entirely closed for all samples. The foaming process was carried out at a constant temperature of 170 °C for 2.25 h at different foaming pressures from 144.26 to 195.74 bar. PLA foams exhibit smaller cell sizes at higher foaming pressures due to increased pressure that hinders cell growth. Additionally, the increased dissolved CO_2 at higher pressures accelerates depressurization and nucleation rates, further reducing cell size [59]. Consistent with our findings, Dugad *et al*. [60] observed a decrease in cell size with increasing pressure due to enhanced cell nucleation and, in turn, a greater density of cells. Our findings also reveal that a further increase in the foaming pressure from 170 to 195.74 bar generates the largest cell size at 24.2 μm. Zhang *et al*. [61] observed a similar trend of increasing cell size with increasing pressure, attributed to reduced cell collapse and enhanced nucleation during depressurization. The cell sizes of 19.8 μm (low pressure), 15.1 μm (mid pressure), and 24.2 μm (high pressure) observed in this study confirm that the foams obtained under the conditions described in Figure 4 are microcellular [6], [7].

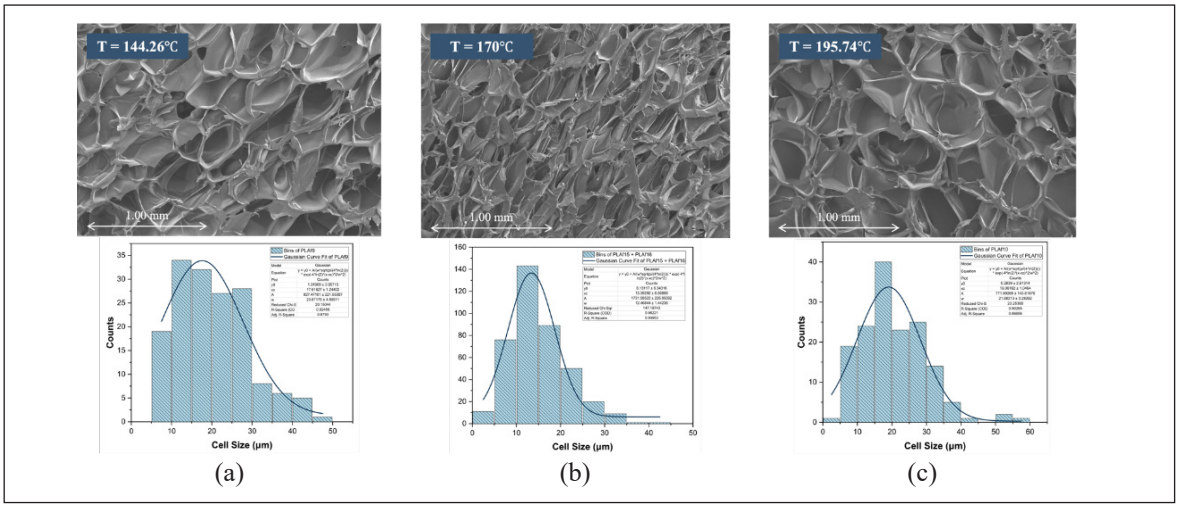

Figure 3: SEM images of the samples foamed at a pressure of 170 bar for 2.25 h (top) and Gaussian curve fit of the cell size distribution (bottom): Variation of foaming temperature.

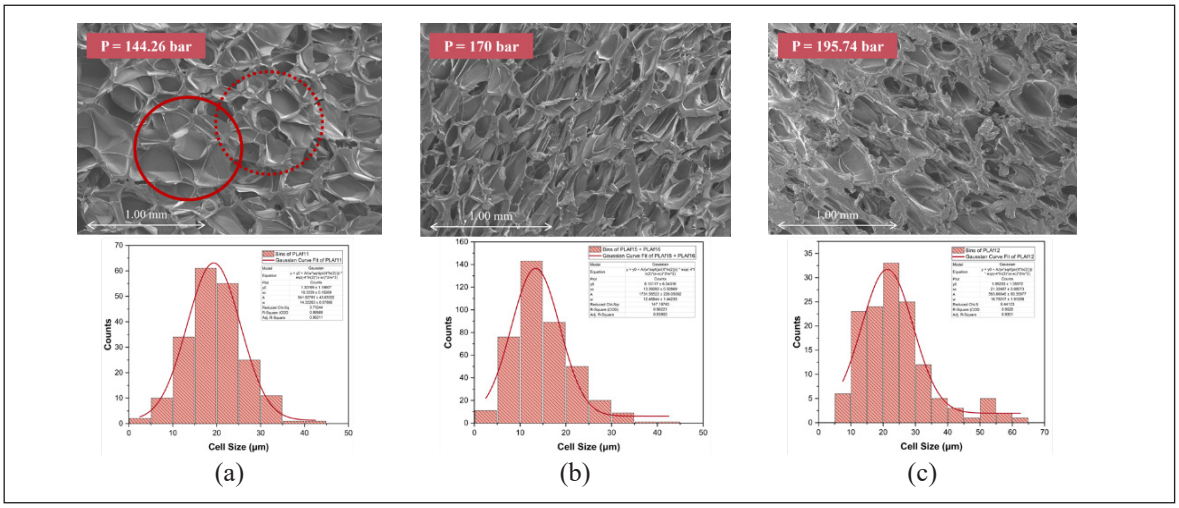

Figure 4: SEM images of the samples foamed at 170 °C for 2.25 h (top) and Gaussian curve fit of the cell size distribution (bottom): Variation of foaming pressure.

The effect of foaming time on the cell morphology and size distribution of the PLA foams was also examined. The cell morphology of the samples prepared at 170 °C and 170 bar for varying foaming times ranging from 1.28 to 3.22 h is compared in Figure 5. Initially, the cell size decreases with increasing time but then increases at longer times due to enhanced gas escape before solidification [62]. However, increased cell size at prolonged foaming time beyond a certain limit leads to continual growth of the cells and the coalescence of cells close to one another. Similar to the findings of Daryadel *et al*. [63], the initial decrease in cell size is attributed to gas consumption for nucleation, leaving less for cell growth. Sundarram *et al*. [17] observed a similar trend of oscillating cell size, with cell size measurements increasing initially due to post-expansion foaming during sample cooling in the hot vessel. This reheating, caused by the thermal inertia of the steel walls and the constant heating of the vessel, continues until the sample reaches atmospheric pressure [64].

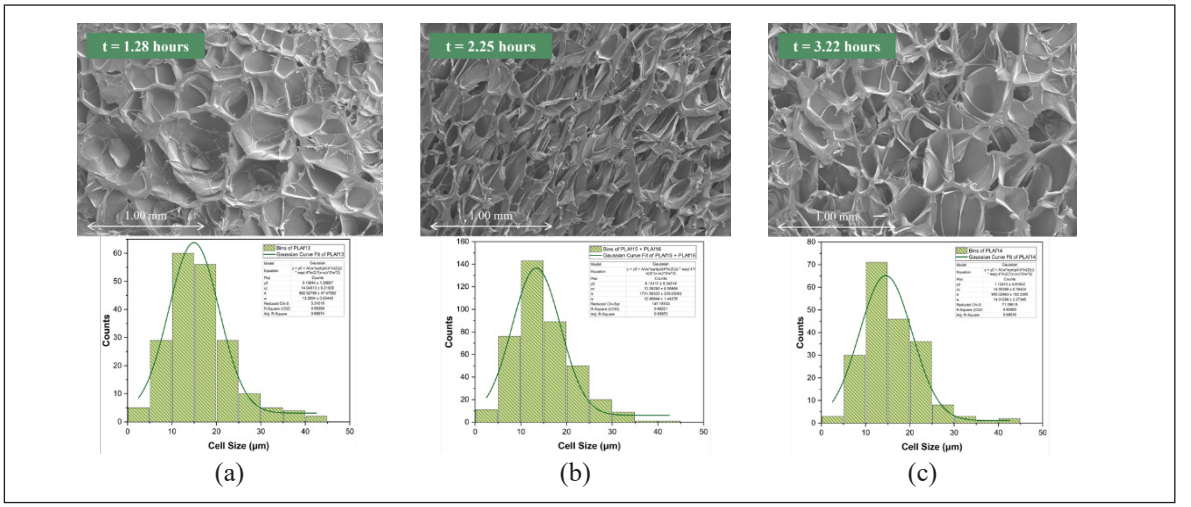

Figure 5: SEM images of the samples foamed at 170 °C and 170 bar (top) and Gaussian curve fit of the cell size distribution (bottom): Variation of foaming time.

3.2 *Effect of single parameter on apparent density, foaming ratio, and cell density*

The effect of a single input parameter change (temperature, pressure, and time) on the properties of the PLA foams was investigated by adjusting a single parameter at a time while keeping the other two parameters constant. Figure 6 shows the relationship between the foaming temperature, apparent density, foaming ratio, cell size, and cell density for particular samples. The apparent density depicted in Figure 6(a) increased with an increase in temperature due to decreased polymer viscosity, leading to cell collapse [65]. Meanwhile, the foaming ratio decreased because of enhanced gas diffusion at higher temperatures [60], [62]. Figure 6(b) demonstrates an inverse relationship between cell size and density. As the cell size decreased, cell density increased due to increased accessible volume within the foam [66]. The cell growth rate initially decreased as the cell density increased and the melt strength increased [62], [67]. However, at higher temperatures, the cell density decreases due to a rise in the cell growth rate, which leads to a decrease in the cell nucleation rate [60].

The impact of foaming pressure on various parameters is illustrated in Figure 7. Increasing foaming pressure has the same effect as increasing foaming temperature on these parameters. Higher gas solubility with increasing pressure leads to increased apparent

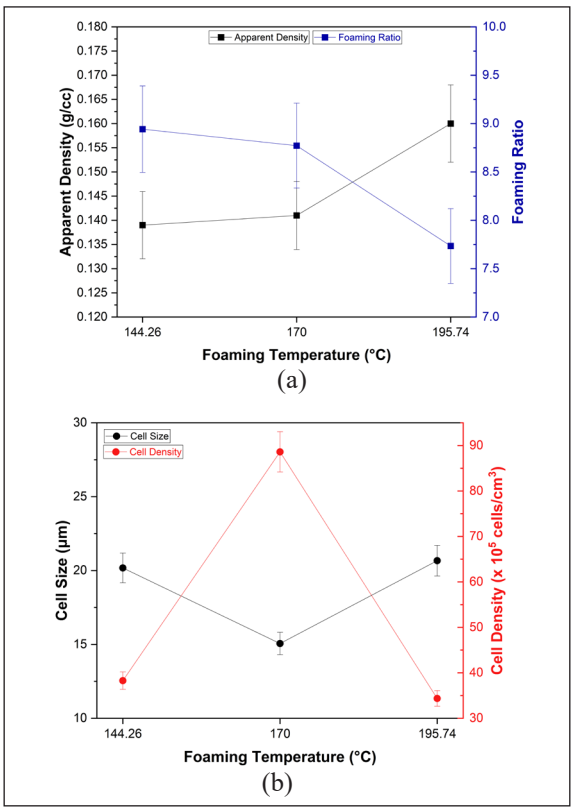

Figure 6: Effect of foaming temperature on the responses with a fixed pressure of 170 bar for 2.25 h: (a) apparent density vs. foaming ratio, and (b) cell size vs. cell density.

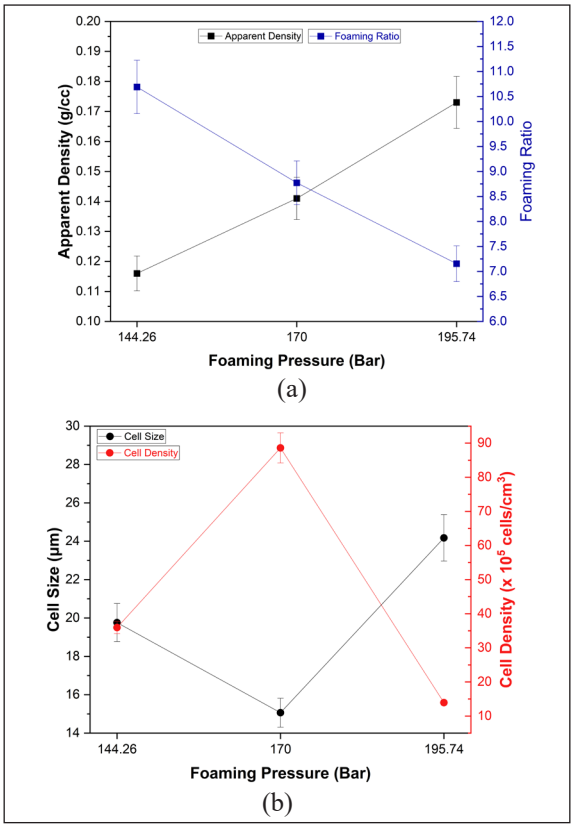

Figure 7: Effect of foaming pressure on the responses with a fixed temperature of 170 ℃ for 2.25 h: (a) apparent density vs. foaming ratio, and (b) cell size vs. cell density

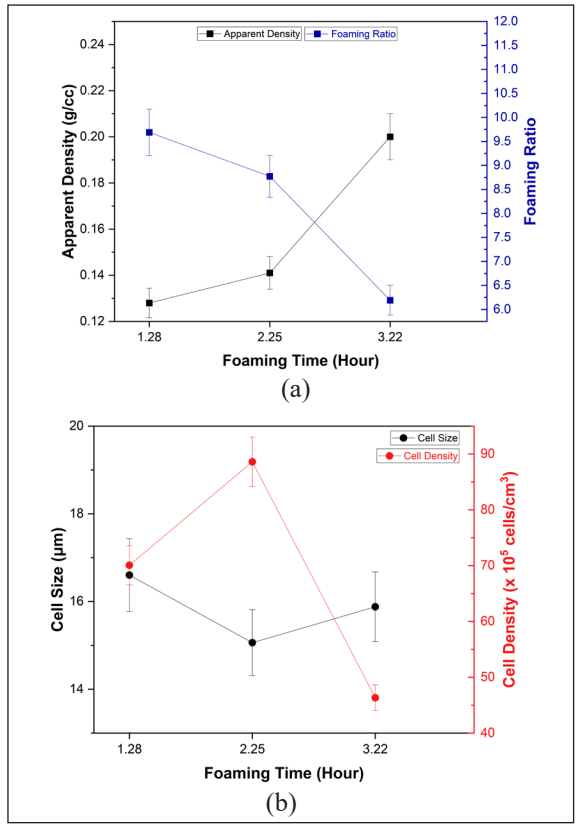

Figure 8: Effect of foaming time on the responses with a fixed condition of 170 ℃ and 170 bar: (a) apparent density vs. foaming ratio, and (b) cell size vs. cell density.

density and cell density [68], but a decreased foaming ratio due to enhanced gas diffusion [69]. However, cell rupture at the highest pressure of 195.75 bar results in larger cell sizes and lower cell densities due to the excessive dissolved gas [70].

In addition, the effect of exposure time to the blowing agent on the foam structures and properties is investigated. Figure 8 shows that the apparent density positively correlates with the foaming time and is inversely related to the foaming ratio. Increasing foaming time initially led to higher apparent density and cell density due to increased cell formation and growth [63]. However, prolonged foaming time resulted in cell collapse and reduced cell density due to polymer stiffening, preventing cell growth, which causes a decrease in the foaming ratio and increases the apparent density [71].

3.3 *Compressive properties*

Figures 9(a), 10(a), and 11(a) illustrate the characteristic three-stage stress-strain curves of specific foamed samples: low-strain linear elasticity, stress plateau, and foam densification. Regional variations in the compressive modulus of neat PLA foams are visually summarized in Supplemental Figure S1, reflecting the influence of different processing conditions on their mechanical behavior. Region 1 shows the foam's elastic stiffness, characterized by a linear relationship between stress and strain. Region 2 demonstrates the collapse of the foam structure beyond a yield point through substantial deformation while maintaining a relatively constant stress, reflected by a much lower compressive modulus than Region 1. Region 3 represents the foam densification after all cells

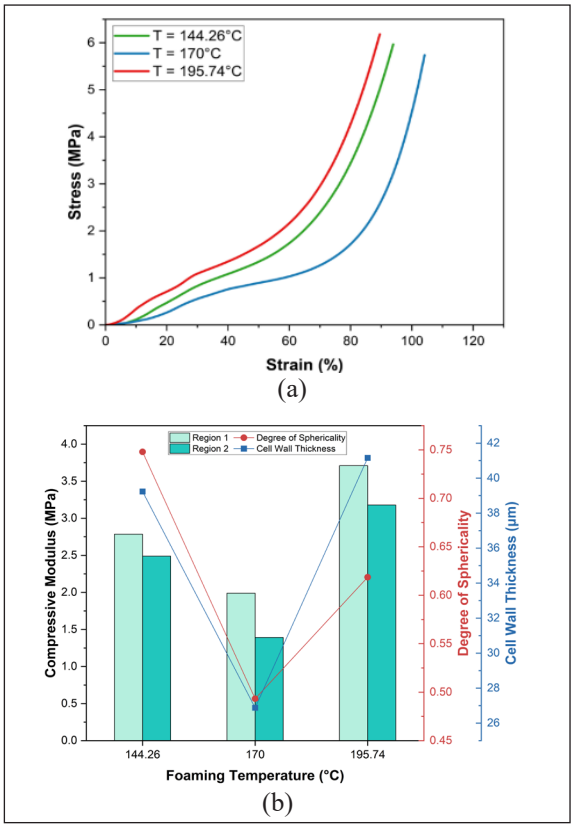

Figure 9: Effect of foaming temperature on the responses: (a) compressive stress-strain curve, and (b) compressive modulus vs. cell size and cell density.

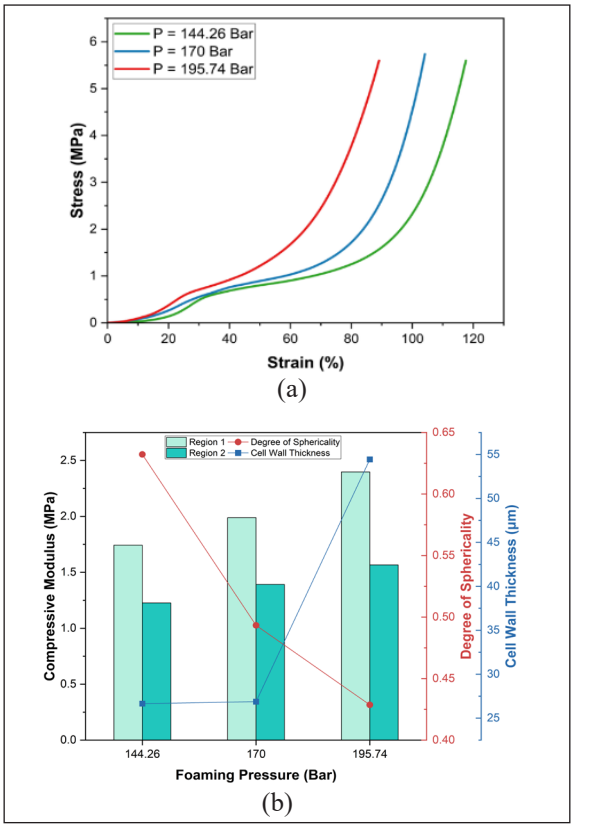

Figure 10: Effect of foaming pressure on the responses: (a) compressive stress-strain curve, and (b) compressive modulus vs. cell size and cell density.

completely collapsed, characterized by the highest compressive modulus and rapid stress increase. The modulus in Region 3 from all stress-strain curves is significantly consistent, reflecting the nature of similar dense PLA material. The corresponding values from Regions 1 and 2 were closely examined to investigate the difference in mechanical properties displayed by the foams in these crucial regions.

Figure 9(b) shows that increasing foaming temperature initially results in decreased compressive modulus, attributed to lower sphericality (observed in Figure 3(b)). Irregularly shaped cells are vulnerable to buckling and collapsing under compressive deformation due to higher stress concentrations at enlarged surface areas or sharp corners in the non-spherical ones [72], [73]. However, there is a subsequent increase in compressive modulus at the highest foaming temperatures due to higher sphericality and thicker cell walls. High sphericality minimizes the risk of cell collapse by distributing stress evenly across cell surfaces [74]. Simultaneously, thicker cell walls enhance the foam's resistance to load compression by reducing its sensitivity to both fracture and buckling [75].

Figure 10(b) shows that higher foaming pressure results in higher compressive modulus. Although higher pressure reduces sphericality, it promotes thicker cell walls, as evidenced by SEM images (Figure 4(c)). These thicker walls enhance the foam's resistance to deformation, as demonstrated by the higher plateaus in the stress-strain curves of Figure 11(a). These plateaus indicate greater resistance to buckling and collapse associated with thicker walls [75]. The cell wall thickness and degree of sphericality were determined by averaging measurements from three distinct regions.

Similar to temperature dependence, the foaming time in Figure 11(b) significantly influences compressive

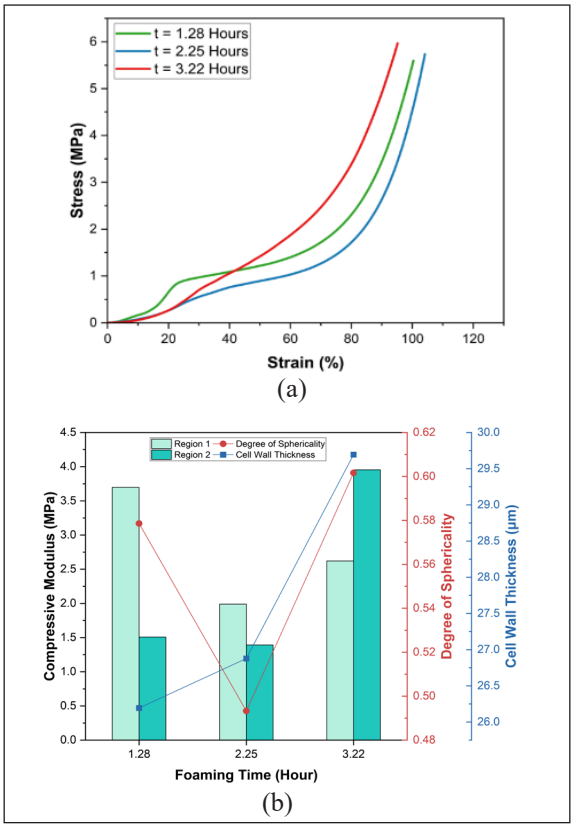

Figure 11: Effect of foaming time on the responses: (a) compressive stress-strain curve, and (b) compressive modulus vs. cell size and cell density.

modulus to fluctuate. However, unlike temperature, longer times promote thickened cell walls, potentially contributing to this effect. The highest compressive modulus observed for the shortest foaming time and lower cell wall thickness might be related to the double peak in region 1 of the stress-strain curve (green line) in Figure 12(a). These distinct peaks suggest cell non-uniformity, confirmed by the bell-shaped distribution in the SEM images and Gaussian curve fit of Figure 5(a). The first peak in the stress-strain curve likely represents earlier cell collapse due to a lower degree of sphericality. In contrast, the second peak indicates a temporary resistance to collapse before entering Region 2. Further increases in foaming time led to higher compressive moduli, as evidenced by the stress-strain curve of the sample foamed for 3.22 h (red line). This curve exhibits a continuous rise in stress without a plateau, suggesting a more robust structure

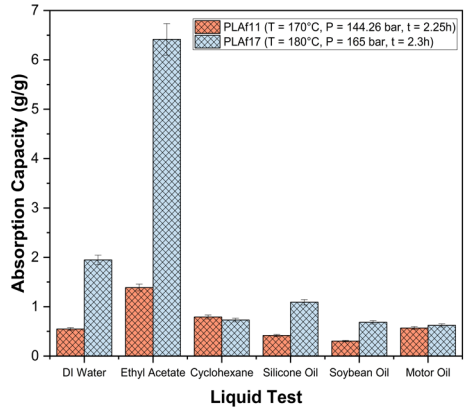

Figure 12: The average absorption capacity of PLAf11 and PLAf17 foam samples toward different organic liquids/oils from three cycles of measurements.

that resists significant cell collapse and buckling under compression. This enhanced stability is likely attributed to thicker and stronger cell walls, resulting in a more pronounced rise in stress with increasing strain. Consequently, the compressive modulus in Region 2 surpasses that of Region 1 for the 3.22-h sample.

3.4 *Model fitting and statistical analysis*

The CCD experimental data were used for statistical analysis, emphasizing the relationship between temperature, pressure, and time. The significance of the regression coefficients was determined by their *p*-values, with lower values indicating higher model significance [76]. All regression models displayed *p*-values below 0.05 [77], affirming their significance at a 5% confidence level, as indicated in Supplemental Table S1 through ANOVA results. The lack-of-fit test verified that all models fitted the data well, with F-values above 0.05 indicating statistical insignificance. To make the models suit, an insignificant value of lack-of-fit is necessary [78]. In these polynomial equations, positive coefficients signify an increase in the related response, while negative coefficients indicate the opposite effect.

Supplemental Figure S2 displays diagnostic plots providing insights into model fitting, reliability, and the correlation between predicted and actual values. Minor deviations from a straight line, despite R-square values not being precisely 1.00 for all responses, suggest a close agreement between the predicted

and actual values. The linear curve fit indicates a significant similarity between the two values, validating the regression model's reliability. These findings confirm that this experimental design is a reliable starting point for future polymeric foaming process design.

3.5 *Process optimization and model validation*

The desirability profiler is used to determine the optimal process conditions by minimizing apparent density, keeping compressive modulus and cell density within range, and minimizing cell size. As summarized in Supplemental Figure S3, the results indicate that the optimal conditions for producing PLA foams *via* solid-state batch foaming with a supercritical CO_2 blowing agent are 180 °C, 165 bar, and 2.3 h. The predicted values achieved by the optimized foaming process conditions are extremely near to the desired level of 0.930 out of 1. The accuracy of the predicted values obtained from the desirability profiler was confirmed by conducting three replicated trials under the optimal conditions suggested by the numerical solutions generated by the software. The data, as summarized in Table 2, show that all responses' predicted and experimental values are slightly different, with a relative deviation of less than 10%. This confirms the model's accuracy and indicates a good correlation between the observed and predicted values [79].

3.6 *Absorption performance and surface wettability*

A promising use of polymeric foams derived from biopolymers is absorbent, especially in biomedical and environmental applications. The mean value of absorption capacity is depicted in Figure 12. PLAf17 outperformed PLAf11 in absorption due to its smaller cell size. These smaller cells of PLAf17 offer increased foam boundaries and interfaces, allowing more liquid entry and spread, resulting in higher absorption capacity [80], [81]. Supplemental Figure S4 shows the solubility parameters (δ_p) of PLA and test liquids/oil [82]–[88]. The δ_p values closer to that of PLA indicate higher miscibility between the liquid and the foam, leading to enhanced absorptivity. Ethyl acetate exhibits the highest absorption capacity due to its similar δ_p value to PLA, improving wetting and penetration [89], [90]. Conversely, DI water's δ_p value is significantly different from PLA. This limits its absorption, causing its molecules to clump together rather than interact with the foam's hydrophobic surface [91], [92].

Figure 13 demonstrates that the superior early absorption exhibited by PLAf17 can be attributed to its higher surface area, a consequence of its smaller cell size. However, a significant rise in absorption is observed for both foams upon the onset of liquid penetration into the internal structure [93], [94]. The measurements of the surface wettability and absorption rates for different liquids/oils involved dropping 20 µL samples onto PLA foams, as summarized in Supplemental Figures S5 and S6. As shown in Supplemental Figure S5, ethyl acetate spreads effortlessly on the surface, forming no droplets. This reflects its low surface tension, confirmed by the 0° contact angle and supported by a close match of its δ_p value with PLA. This close match encourages stronger interactions, reducing contact angles and enhancing wetting [95]. Despite a δ_p mismatch with PLA, motor oil also avoids forming droplets, highlighting the foam's lipophilic and hydrophobic nature. The smaller cell size of PLAf17 seems to create a more uniform, less hydrophobic surface, leading to efficient liquid wetting and a lower contact angle than PLAf11 [96]. As evidenced in Supplemental Figure S6, ethyl acetate dominates the absorption rate for both PLA foams, followed by the other liquids. DI water, hindered by the foam's hydrophobicity, struggles significantly. Interestingly, the smaller cell size of PLAf17 translates to faster absorption across all liquids, echoing findings by Ding *et al*. [97], who observed similar behavior in modified PLA foams with smaller cells.

Table 2: Model validation of predicted foaming process conditions

Values	Input Parameters				Output Responses		
	T (°C)	P (bar)	t (hour)	Apparent Density (g/cc)	Compressive Modulus (MPa)	Average Cell Size (µm)	Cell Density ($\times 10^5$ cells/cc)
Predicted	180	165	2.3	0.135	1.99	19.1	51.0
Experimental				0.134	1.96	21.1	52.4
Relative deviation (%)				**0.793**	**1.81**	**9.2**	**2.7**

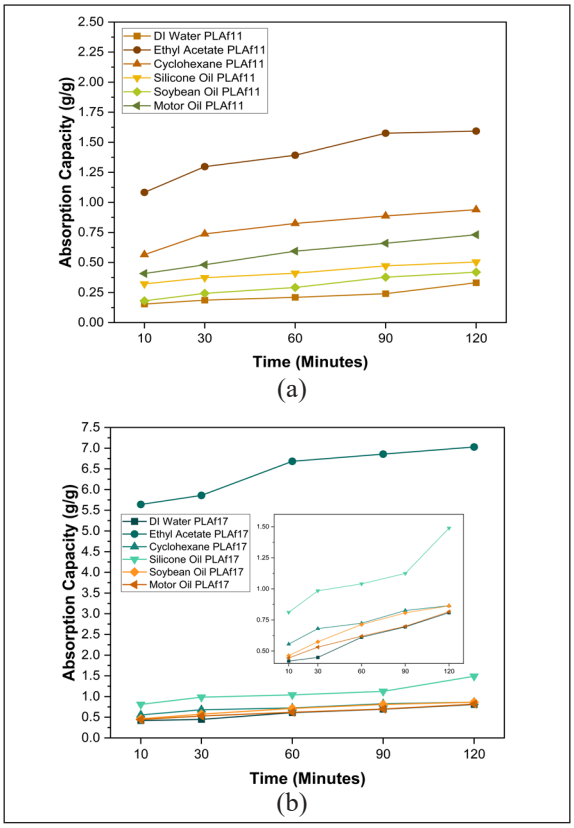

Figure 13: Mean values of absorption capacity for selected PLA foam samples were observed over three absorption cycles with different test liquids as a function of absorption time: (a) PLAf11 and (b) PLAf17.

4 Conclusions

A fabrication process of PLA foams using the solid-state batch foaming method with supercritical CO_2 as a physical blowing agent has been developed to obtain foams with optimal cell morphology and properties. The central composite design of response surface methodology was utilized as the baseline for the design of experiment to analyze the effect of various process parameters on the foams' cell structures and properties. The findings revealed that it is possible to obtain PLA foams with desired cell structures and properties by controlling the foaming temperature, pressure, and time. The cell size distribution of all samples is roughly bell-shaped and categorized as microcellular foam. The apparent density of the foams is inversely proportional to the foaming ratio at three levels of process parameters. However, the cell size is directly proportional to the apparent density at initial levels of process parameters. After passing the optimum level, cell size is inversely proportional to apparent density. The same relationship was observed between the cell and apparent density but in the opposite direction.

The compressive modulus follows a typical three-stage stress-strain behavior pattern. Both foaming temperature and time controlled the compressive modulus. Higher levels of these parameters initially resulted in a decrease in compressive modulus at 50% strain, but subsequent increases resulted in the highest value of compressive modulus. In contrast, higher foaming pressure resulted in a higher compressive modulus. The response surface analysis provided insights into how these parameters interact and influence apparent density, compressive modulus, cell size, and cell density. The close alignment between the predicted and experimental values confirms the model's accuracy. Improved efficiency and consistency in fabricating PLA foams can be achieved with the help of this model. This study also investigated the ability of the foams to absorb different liquids. This finding highlights the potential of PLA foams as absorbents and broadens our understanding of their usefulness beyond their cell morphology. Future research should prioritize optimizing the foaming process with specific methods for diverse industrial needs to broaden the use of foamed PLA further. However, significant challenges remain in scaling production and ensuring sustainable end-of-life management, especially considering the high PLA consumption.

Acknowledgments

The authors are grateful for the support from the Thailand Science Research and Innovation Fundamental Fund (through Thammasat University), the Center of Excellence in Functional Advanced Materials Engineering (CoE FAME), Thammasat University, and the National Metal and Materials Technology Center (MTEC), Thailand. Y.A.Y. acknowledges the Excellent Foreign Student (EFS) scholarship provided by SIIT.

Author Contributions

Y.A.Y. designed and performed all experiments, analyzed and visualized data, and authored the initial draft;

A.P. guided the field experiment implementation; P.O. (corresponding author) masterminded the experiment, secured funding, supervision its execution, and ensured manuscript accuracy through review and editing.

Conflicts of Interest

The authors declare no conflict of interest.

References

[1] F. L. Jin, M. Zhao, M. Park, and S. J. Park, "Recent trends of foaming in polymer processing: A review," *Polymers (Basel)*, vol. 11, no. 6, p. 953, 2019, doi: 10.3390/polym11060953.

[2] S. Sumardiono, I. Pudjihastuti, R. Amalia, and Y. A. Yudanto, "Characteristics of biodegradable foam (bio-foam) made from cassava flour and corn fiber," in *IOP Conference Series: Materials Science and Engineering*, 2021, Art. no. 1053.

[3] Y. A. Yudanto and I. Pudjihastuti, "Characterization of physical and mechanical properties of Biodegradable foam from maizena flour and paper waste for Sustainable packaging material," *International Journal of Engineering Applied Sciences and Technology*, vol. 5, no. 8, pp. 1–8, 2020.

[4] J. G. Drobny, "Processing methods applicable to thermoplastic elastomers," in *Handbook of Thermoplastic Elastomers*, J. G. Drobny, Ed. Oxford, UK: William Andrew Publishing, pp. 33–173, 2014.

[5] M. A. Osman, N. Virgilio, M. Rouabhia, and F. Mighri, "Polylactic acid (PLA) foaming: Design of experiments for cell size control," *Materials Sciences and Applications*, vol. 13, no. 2, pp. 63–77, 2022.

[6] M. Nofar and C. B. Park, "1 - Introduction to plastic foams and their foaming," in *Polylactide Foams*, M. Nofar and C. B. Park, Eds. New York: William Andrew Publishing, pp. 1–16, 2018.

[7] J. Chen, L. Yang, D. Chen, Q. Mai, M. Wang, L. Wu, and P. Kong, "Cell structure and mechanical properties of microcellular PLA foams prepared *via* autoclave constrained foaming," *Cellular Polymers*, vol. 40, no. 3, pp. 101–118, 2021.

[8] X. Wei, J. Luo, X. Wang, H. Zhou, and Y. Pang, "ScCO_2-assisted fabrication and compressive property of poly (lactic acid) foam reinforced by in-situ polytetrafluoroethylene fibrils," *International Journal of Biological Macromolecules*, vol. 209, pp. 2050–2060, 2022.

[9] W. Li, Q. Ren, X. Zhu, M. Wu, Z. Weng, L. Wang, and W. Zheng, "Enhanced heat resistance and compression strength of microcellular poly (lactic acid) foam by promoted stereocomplex crystallization with added D-Mannitol," *Journal of CO_2 Utilization*, vol. 63, 2022, Art. no. 102118.

[10] L. J. Jia, A. D. Phule, Z. Yu, X. Zhang, and Z. X. Zhang, "Ultra-light poly (lactic acid)/SiO_2 aerogel composite foam: A fully biodegradable and full life-cycle sustainable insulation material," *International Journal of Biological Macromolecules*, vol. 192, pp. 1029–1039, 2021.

[11] Y. Wang, F. Guo, X. Liao, S. Li, Z. Yan, F. Zou, Q. Peng, and G. Li, "High-expansion-ratio PLLA/PDLA/HNT composite foams with good thermally insulating property and enhanced compression performance *via* supercritical CO_2," *International Journal of Biological Macromolecules*, 2023, Art. no. 123961.

[12] T. Song, M. Liu, J. Tian, S. Wang, and Q. Li, "Effect of PLA/TiO_2/Lg filler competition and synergy on crystallization behavior, mechanics and functionality of composite foaming materials," *Polymer*, vol. 271, 2023, Art. no. 125797.

[13] K. Bocz, T. Tábi, D. Vadas, M. Sauceau, J. Fages, and G. Marosi, "Characterisation of natural fibre reinforced PLA foams prepared by supercritical CO_2 assisted extrusion," *Express Polymer Letters*, vol. 10, no. 9, pp. 771–779, 2016.

[14] K. Oluwabunmi, N. A. D'Souza, W. Zhao, T.-Y. Choi, and T. Theyson, "Compostable, fully biobased foams using PLA and micro cellulose for zero energy buildings," *Scientific Reports*, vol. 10, no. 1, pp. 1–20, 2020.

[15] S. G. Mosanenzadeh, H. E. Naguib, C. B. Park, and N. Atalla, "Development, characterization, and modeling of environmentally friendly open-cell acoustic foams," *Polymer Engineering & Science*, vol. 53, no. 9, pp. 1979–1989, 2013.

[16] Y. Shimazaki, S. Nozu, and T. Inoue, "Shock-absorption properties of functionally graded EVA laminates for footwear design," *Polymer Testing*, vol. 54, pp. 98–103, 2016.

[17] S. S. Sundarram, N. Ibekwe, S. Prado, C. Rotonto,

and S. Feeney, "Microwave foaming of carbon dioxide saturated poly lactic acid," *Polymer Engineering & Science*, vol. 62, no. 3, pp. 929–938, 2022.

[18] B. Notario, J. Pinto, and M. A. Rodriguez-Perez, "Nanoporous polymeric materials: A new class of materials with enhanced properties," *Progress in Materials Science*, vol. 78, pp. 93–139, 2016.

[19] M. A. Alim, M. Moniruzzaman, M. M. Hossain, Wahiduzzaman, M. R. Repon, I. Hossain, and M. A. Jalil, "Manufacturing and compatibilization of binary blends of superheated steam treated jute and poly (lactic acid) biocomposites by melt-blending technique," *Heliyon*, vol. 8, no. 8, 2022, Art. no. e09923.

[20] A. Jalali, J.-H. Kim, A. M. Zolali, I. Soltani, M. Nofar, E. Behzadfar, and C. B. Park, "Peculiar crystallization and viscoelastic properties of polylactide/polytetrafluoroethylene composites induced by in-situ formed 3D nanofiber network," *Composites Part B: Engineering*, vol. 200, 2020, Art. no. 108361.

[21] O. D. Putri, A. Petchsuk, S. Bayram, and P. Opaprakasit, "Ultrasonicate-assisted preparation of eumelanin-loaded nano/microparticles based on polylactide stereocomplex," *Materials Today: Proceedings*, vol. 66, pp. 3025–3030, 2022.

[22] K. Thananukul, C. Kaewsaneha, P. Sreearunothai, A. Petchsuk, S. Buchatip, W. Supmak, B. Nim, M. Okubo, and P. Opaprakasit, "Biocompatible degradable hollow nanoparticles from curable copolymers of polylactic acid for uv-shielding cosmetics," *ACS Applied Nano Materials*, vol. 5, no. 3, pp. 4473–4483, 2022.

[23] K. Pleejaroen, D. Yiamsawas, and P. Opaprakasit, "In-situ synthesis of Lignin/ZnO composites from black liquor for uv-resistant and antioxidant agents in bioplastics," *SIAM: Science and Innovation of Advanced Materials*, vol. 3, no. 1, pp. 66002-1–66002-9, 2023.

[24] B. Nim, S. S. Rahayu, K. Thananukul, C. Eang, M. Opaprakasit, A. Petchsuk, C. Kaewsaneha, D. Polpanich, and P. Opaprakasit, "Sizing down and functionalizing polylactide (PLA) resin for synthesis of PLA-based polyurethanes for use in biomedical applications," *Scientific Reports*, vol. 13, no. 1, p. 2284, 2023.

[25] C. Eang, B. Nim, M. Opaprakasit, A. Petchsuk, and P. Opaprakasit, "Polyester-based polyurethanes derived from alcoholysis of polylactide as toughening agents for blends with shape-memory properties," *RSC Advances*, vol. 12, no. 54, pp. 35328–35340, 2022.

[26] B. Nim and P. Opaprakasit, "Quantitative analyses of products from chemical recycling of polylactide (PLA) by alcoholysis with various alcohols and their applications as healable lactide-based polyurethanes," *Spectrochimica Acta Part A: Molecular and Biomolecular Spectroscopy*, vol. 255, 2021, Art. no. 119684.

[27] B. Nim, M. Opaprakasit, A. Petchsuk, and P. Opaprakasit, "Microwave-assisted chemical recycling of polylactide (PLA) by alcoholysis with various diols," *Polymer Degradation and Stability*, vol. 181, 2020, Art. no. 109363.

[28] N. Jaikaew, R. Auras, and P. Opaprakasit, "Optimization of melt-mixing transesterification of polylactide by polyethylene glycol employing response surface methodology," *Chiang Mai Journal of Science*, vol. 49, no. 1, pp. 69–80, 2022.

[29] C. Eang, B. Nim, P. Sreearunothai, A. Petchsuk, and P. Opaprakasit, "Chemical upcycling of polylactide (PLA) and its use in fabricating PLA-based super-hydrophobic and oleophilic electrospun nanofibers for oil absorption and oil/water separation," *New Journal of Chemistry*, vol. 46, no. 31, pp. 14933–14943, 2022, doi: 202210.1039/D2NJ02747J.

[30] C. Eang and P. Opaprakasit, "Electrospun nanofibers with superhydrophobicity derived from degradable polylactide for oil/water separation applications," *Journal of Polymers and the Environment*, vol. 28, no. 5, pp. 1484–1491, 2020.

[31] T. P. P. Le and P. Opaprakasit, "Preparation of polylactide/modified clay bio-composites employing quaternized chitosan-modified montmorillonite clays for use as packaging films," *CET Journal-Chemical Engineering Transactions*, vol. 78, 2020, doi: 10.3303/CET2078020.

[32] S. Farah, D. G. Anderson, and R. Langer, "Physical and mechanical properties of PLA, and their functions in widespread applications — A comprehensive review," *Advanced Drug Delivery Reviews*, vol. 107, pp. 367–392, 2016.

[33] Y. Wang, F. Guo, X. Liao, S. Li, Z. Yan, F. Zou, Q. Peng, and G. Li, "High-expansion-ratio PLLA/PDLA/HNT composite foams with good thermally insulating property and enhanced compression performance *via* supercritical CO_2," *International Journal of Biological Macromolecules*, vol. 236, 2023, Art. no. 123961.

[34] E. Di Maio, S. Iannace, and G. Mensitieri, "Foams and their applications," in *Supercritical Fluid Science and Technology*. Amsterdam, Netherlands: Elsevier, pp. 1–20, 2021.

[35] Q. Ren, X. Zhu, W. Li, M. Wu, S. Cui, Y. Ling, X. Ma, G. Wang, L. Wang, and W. Zheng, "Fabrication of super-hydrophilic and highly open-porous poly (lactic acid) scaffolds using supercritical carbon dioxide foaming," *International Journal of Biological Macromolecules*, vol. 205, pp. 740–748, 2022.

[36] F. Zou, X. Liao, P. Song, S. Shi, J. Chen, X. Wang, and G. Li, "Enhancement of electrical conductivity and electromagnetic interference shielding performance *via* supercritical CO_2 induced phase coarsening for double percolated polymer blends," *Nano Research*, vol. 16, no. 1, pp. 613–623, 2023.

[37] Y. A. Yudanto and P. Opaprakasit, "A Preliminary Review of Poly(lactic acid)-based Biodegradable Foam and its Techno-economic Model," *E3S Web of Conferences*, vol. 448, 2023, Art. no. 03076.

[38] M. C. Macawile and J. Auresenia, "Utilization of supercritical carbon dioxide and co-solvent n-hexane to optimize oil extraction from gliricidia sepium seeds for biodiesel production," *Applied Science and Engineering Progress*, vol. 15, no. 1, 2022, Art. no. 5404, doi: 10.14416/j.asep.2021.09.003.

[39] L. Geng, L. Li, H. Mi, B. Chen, P. Sharma, H. Ma, B. S. Hsiao, X. Peng, and T. Kuang, "Superior impact toughness and excellent storage modulus of poly(lactic acid) foams reinforced by shish-kebab nanoporous structure," *ACS Applied Materials & Interfaces*, vol. 9, no. 25, pp. 21071–21076, 2017.

[40] W. Ding, D. Jahani, E. Chang, A. Alemdar, C. B. Park, and M. Sain, "Development of PLA/cellulosic fiber composite foams using injection molding: Crystallization and foaming behaviors," *Composites Part A: Applied Science and Manufacturing*, vol. 83, pp. 130–139, 2016.

[41] D. Xu, K. Yu, K. Qian, and C. B. Park, "Foaming behavior of microcellular poly(lactic acid)/TPU composites in supercritical CO_2," *Journal of Thermoplastic Composite Materials*, vol. 31, no. 1, pp. 61–78, 2018, doi: 10.1177/0892705716679480.

[42] Z. Han, Y. Zhang, W. Yang, and P. Xie, "Advances in microcellular foam processing of PLA," *Key Engineering Materials*, vol. 717, pp. 68–72, 11/01 2016.

[43] M. Mahdavi, O. Yousefzade, and H. Garmabi, "A simple method for preparation of microcellular PLA/calcium carbonate nanocomposite using super critical nitrogen as a blowing agent: Control of microstructure," *Advances in Polymer Technology*, vol. 37, no. 8, pp. 3017–3026, 2018.

[44] H. Haham, A. Riscoe, C. W. Frank, and S. L. Billington, "Effect of bubble nucleating agents derived from biochar on the foaming mechanism of poly lactic acid foams," *Applied Surface Science Advances*, vol. 3, 2021, Art. no. 100059.

[45] E. Di Maio, S. Iannace, and G. Mensitieri, "Chapter 13 - Batch processing," in *Supercritical Fluid Science and Technology*, vol. 9, E. Di Maio, S. Iannace, and G. Mensitieri, Eds. Amsterdam, Netherlands: Elsevier, pp. 389–410, 2021.

[46] A. N. Frone, D. M. Panaitescu, I. Chiulan, C. A. Nicolae, Z. Vuluga, C. Vitelaru, and C. M. Damian, "The effect of cellulose nanofibers on the crystallinity and nanostructure of poly (lactic acid) composites," *Journal of Materials Science*, vol. 51, pp. 9771–9791, 2016.

[47] C. Fan, C. Wan, F. Gao, C. Huang, Z. Xi, Z. Xu, L. Zhao, and T. Liu, "Extrusion foaming of poly (ethylene terephthalate) with carbon dioxide based on rheology analysis," *Journal of Cellular Plastics*, vol. 52, no. 3, pp. 277–298, 2016.

[48] *D792-20 Standard Test Methods for Density and Specific Gravity (Relative Density) of Plastics by Displacement*, ASTM International, 2020.

[49] *ASTM D695-15 Standard Test Method for Compressive Properties Rigid Plastics*, ASTM International, 2015.

[50] *ASTM D570-98 Standard Test Method for Water Absorption of Plastics*, ASTM International, 2018.

[51] M. Q. Seah, Z. C. Ng, W. J. Lau, M. Gürsoy,

M. Karaman, T.-W. Wong, and A. F. Ismail, "Development of surface modified PU foam with improved oil absorption and reusability *via* an environmentally friendly and rapid pathway," *Journal of Environmental Chemical Engineering*, vol. 10, no. 1, 2022, Art. no. 106817.

[52] W. Xiao, B. Niu, M. Yu, C. Sun, L. Wang, L. Zhou, and Y. Zheng, "Fabrication of foam-like oil sorbent from polylactic acid and Calotropis gigantea fiber for effective oil absorption," *Journal of Cleaner Production*, vol. 278, 2021, Art. no. 123507.

[53] E. Rostami-Tapeh-Esmaeil and D. Rodrigue, "Morphological, mechanical and thermal properties of rubber foams: A review based on recent investigations," *Materials*, vol. 16, no. 5, 2023, Art. no. 1934.

[54] D. Tammaro, M. M. Villone, G. D'Avino, and P. L. Maffettone, "An experimental and numerical investigation on bubble growth in polymeric foams," *Entropy*, vol. 24, no. 2, p. 183, 2022.

[55] Y. Liu, J. Li, S. Sun, and B. Yu, "Advances in Gaussian random field generation: A review," *Computational Geosciences*, vol. 23, pp. 1011–1047, 2019.

[56] M. Marvi-Mashhadi, C. Lopes, and J. LLorca, "Surrogate models of the influence of the microstructure on the mechanical properties of closed-and open-cell foams," *Journal of Materials Science*, vol. 53, pp. 12937–12948, 2018.

[57] F. Guo, X. Liao, S. Li, Z. Yan, W. Tang, and G. Li, "Heat insulating PLA/HNTs foams with enhanced compression performance fabricated by supercritical carbon dioxide," *The Journal of Supercritical Fluids*, vol. 177, 2021, Art. no. 105344.

[58] Q. Ren, J. Wang, W. Zhai, and R. E. Lee, "Fundamental influences of induced crystallization and phase separation on the foaming behavior of poly (lactic acid)/polyethylene glycol blends blown with compressed CO_2," *Industrial & Engineering Chemistry Research*, vol. 55, no. 49, pp. 12557–12568, 2016.

[59] L. Xu, S. Qian, W. Zheng, Y. Bai, and Y. Zhao, "Formation mechanism and tuning for bimodal open-celled structure of cellulose acetate foams prepared by supercritical CO_2 foaming and poly (ethylene glycol) leaching," *Industrial & Engineering Chemistry Research*, vol. 57, no. 46, pp. 15690–15696, 2018.

[60] R. Dugad, G. Radhakrishna, and A. Gandhi, "Morphological evaluation of ultralow density microcellular foamed composites developed through CO_2-induced solid-state batch foaming technique utilizing water as co-blowing agent," *Cellular Polymers*, vol. 39, no. 4, pp. 141–171, 2020.

[61] Y. Zhang, J. Wang, J. Zhou, J. Sun, and Z. Jiao, "Multi-modal cell structure formation of poly (lactic-co-glycolic acid)/superparamagnetic iron oxide nanoparticles composite scaffolds by supercritical CO_2 varying-temperature foaming," *Polymers for Advanced Technologies*, vol. 33, no. 6, pp. 1906–1915, 2022.

[62] P. Tiwary, C. B. Park, and M. Kontopoulou, "Transition from microcellular to nanocellular PLA foams by controlling viscosity, branching and crystallization," *European Polymer Journal*, vol. 91, pp. 283–296, 2017.

[63] M. Daryadel, T. Azdast, R. Hasanzadeh, and S. Molani, "Simultaneous decision analysis on the structural and mechanical properties of polymeric microcellular nanocomposites foamed using CO_2," *Journal of Applied Polymer Science*, vol. 135, no. 14, 2018, Art. no. 46098.

[64] M. Dippold and H. Ruckdäschel, "Influence of pressure-induced temperature drop on the foaming behavior of amorphous polylactide (PLA) during autoclave foaming with supercritical CO_2," *The Journal of Supercritical Fluids*, vol. 190, 2022, Art. no. 105734.

[65] J. M. Julien, J. C. Bénézet, E. Lafranche, J. C. Quantin, A. Bergeret, M. F. Lacrampe, and P. Krawczak, "Development of poly(lactic acid) cellular materials: Physical and morphological characterizations," *Polymer*, vol. 53, no. 25, pp. 5885–5895, 2012.

[66] T. Azdast and R. Hasanzadeh, "Increasing cell density/decreasing cell size to produce microcellular and nanocellular thermoplastic foams: A review," *Journal of Cellular Plastics*, vol. 57, no. 5, pp. 769–797, 2021.

[67] M. Nofar, Y. Guo, and C. B. Park, "Double crystal melting peak generation for expanded polypropylene bead foam manufacturing,"

Industrial & Engineering Chemistry Research, vol. 52, no. 6, pp. 2297–2303, 2013.

[68] Y. A. Yudanto, A. Petchsuk, and P. Opaprakasit, "Process optimization of pressure-induced autoclave foaming for PLA foams blown by supercritical CO_2 using central composite design of response surface methodology," presented at the 5th International Conference on Chemical Sciences, Yogyakarta, Indonesia, Aug. 8, 2023.

[69] K. B. Venkatesan, S. S. Karkhanis, and L. M. Matuana, "Microcellular foaming of poly(lactic acid) branched with food-grade chain extenders," *Journal of Applied Polymer Science*, vol. 138, no. 29, 2021, Art. no. 50686.

[70] S. Ghanbar, O. Yousefzade, F. Hemmati, and H. Garmabi, "Microstructure and thermal stability of polypropylene/bagasse composite foams: Design of optimum void fraction using response surface methodology," *Journal of Thermoplastic Composite Materials*, vol. 29, no. 6, pp. 799–816, 2016.

[71] W. Zhai, Y. Ko, W. Zhu, A. Wong, and C. B. Park, "A study of the crystallization, melting, and foaming behaviors of polylactic acid in compressed CO_2," *International Journal of Molecular Sciences*, vol. 10, no. 12, pp. 5381–5397, 2009.

[72] X. Yang, W. Wang, L. Yan, Q. Zhang, and T. J. Lu, "Effect of pore morphology on cross-property link for close-celled metallic foams," *Journal of Physics D: Applied Physics*, vol. 49, no. 50, 2016, Art. no. 505301.

[73] N. Wang, X. Chen, E. Maire, P. H. Kamm, Y. Cheng, Y. Li, and F. García-Moreno, "Study on cell deformation of low porosity aluminum foams under quasi-static compression by x-ray tomography," *Advanced Engineering Materials,* vol. 22, no. 10, 2020, Art. no. 2000264.

[74] D. Yang, H. Wang, S. Guo, J. Chen, Y. Xu, D. Lei, J. Sun, L. Wang, J. Jiang, and A. Ma, "Coupling effect of porosity and cell size on the deformation behavior of Al alloy foam under quasi-static compression," *Materials*, vol. 12, no. 6, p. 951, 2019.

[75] K. Güzel, J. C. Zarges, and H. P. Heim, "Effect of cell morphology on flexural behavior of injection-molded microcellular polycarbonate," *Materials (Basel)*, vol. 15, no. 10, 2022, Art. no. 3634.

[76] A. Prasetyaningrum, W. Widayat, B. Jos, R. Ratnawati, T. Riyanto, G. R. Prinanda, B. U. L. Monde, and E. E. Susanto, "Optimization of sequential microwave-ultrasonic-assisted extraction of flavonoid compounds from Moringa oleifera," *Trends in Sciences*, vol. 20, no. 1, pp. 6401–6401, 2023.

[77] S. Pumkrachang, K. Asawarungsaengkul, and P. Chutima, "Multi-objective optimization of UV spot curing technique of slider-suspension attachment process using response surface methodology approach," *Applied Science and Engineering Progress*, vol. 15, no. 4, pp. 5512–5512, 2022.

[78] O. Stamenković, M. Kostić, D. Radosavljević, and V. Veljković, "Comparison of box-behnken, face central composite and full factorial designs in optimization of hempseed oil extraction by n-hexane: A case study," *Periodica Polytechnica Chemical Engineering*, vol. 62, no. 3, 2018, doi: 10.3311/PPch.11448.

[79] A. Sundarsingh, G. V. S. BhagyaRaj, and K. K. Dash, "Modeling and optimization of osmotic dehydration of wax apple slices using adaptive neuro-fuzzy inference system," *Applied Food Research*, vol. 3, no. 2, 2023, Art. no. 100316.

[80] K. V. Udayakumar, P. M. Gore, and B. Kandasubramanian, "Foamed materials for oil-water separation," *Chemical Engineering Journal Advances*, vol. 5, 2021, Art. no. 100076.

[81] I. B. Djemaa, S. Auguste, W. Drenckhan-Andreatta, and S. Andrieux, "Hydrogel foams from liquid foam templates: Properties and optimisation," *Advances in Colloid and Interface Science*, vol. 294, 2021, Art. no. 102478.

[82] C. Hansen and A. Beerbower, *The Kirk-Othmer Encyclopedia of Chemical Technology*, A. Standen, Eds. New York: Interscience, 1971, Supplement Volume.

[83] A. F. Barton, *CRC Handbook of Solubility Parameters and other Cohesion Parameters*. London, UK: Routledge, 2017.

[84] A. Jarray, A. Feichtinger, and E. Scholten, "Linking intermolecular interactions and rheological behaviour in capillary suspensions," *Journal of Colloid and Interface Science*, vol. 627, pp. 415–426, 2022.

[85] M. M. Batista, R. Guirardello, and M. A. Krähenbühl, "Determination of the Hansen solubility parameters of vegetable oils, biodiesel, diesel, and biodiesel–diesel blends," *Journal of the American Oil Chemists' Society*, vol. 92, no. 1, pp. 95–109, 2015.

[86] J. Gardon and J. Teas, *Characterization of Coatings: Physical Techniques*. New York: Marcel Dekker, 1976.

[87] A. Beerbower and J. Dickey, "Advanced methods for predicting elastomer/fluids interactions," *ASLE transactions*, vol. 12, no. 1, pp. 1–20, 1969.

[88] E. Meaurio, E. Sanchez-Rexach, E. Zuza, A. Lejardi, A. del Pilar Sanchez-Camargo, and J.-R. Sarasua, "Predicting miscibility in polymer blends using the Bagley plot: Blends with poly (ethylene oxide)," *Polymer*, vol. 113, pp. 295–309, 2017.

[89] M. Udayakumar, M. Kollár, F. Kristály, M. Leskó, T. Szabó, K. Marossy, I. Tasnádi, and Z. Németh, "Temperature and time dependence of the solvent-induced crystallization of poly (l-lactide)," *Polymers*, vol. 12, no. 5, p. 1065, 2020.

[90] J. R. Cerda, T. Arifi, S. Ayyoubi, P. Knief, M. P. Ballesteros, W. Keeble, E. Barbu, A. M. Healy, A. Lalatsa, and D. R. Serrano, "Personalised 3D printed medicines: Optimising material properties for successful passive diffusion loading of filaments for fused deposition modelling of solid dosage forms," *Pharmaceutics*, vol. 12, no. 4, p. 345, 2020.

[91] T. Karbowiak, F. Debeaufort, D. Champion, and A. Voilley, "Wetting properties at the surface of iota-carrageenan-based edible films," *Journal of Colloid and Interface Science*, vol. 294, no. 2, pp. 400–410, 2006.

[92] J. R. R. Smith, "A contribution of understanding the stability of commercial PLA films for food packaging and its surface modifications," Ph.D. dissertation, Université Bourgogne Franche-Comté, Université d'Udine (Italie), 2017.

[93] J. Khetan, M. Shahinuzzaman, S. Barua, and D. Barua, "Quantitative analysis of the correlation between cell size and cellular uptake of particles," *Biophysical Journal*, vol. 116, no. 2, pp. 347–359, 2019.

[94] E. Rostami-Tapeh-Esmaeil, A. Vahidifar, E. Esmizadeh, and D. Rodrigue, "Chemistry, processing, properties, and applications of rubber foams," *Polymers*, vol. 13, no. 10, p. 1565, 2021.

[95] N. AlQasas, A. Eskhan, and D. Johnson, "Hansen solubility parameters from surface measurements: A comparison of different methods," *Surfaces and Interfaces*, vol. 36, 2023, Art. no. 102594.

[96] Q. Zheng and C. Lü, "Size effects of surface roughness to superhydrophobicity," *Procedia IUtam*, vol. 10, pp. 462–475, 2014.

[97] M. M. Hassan, M. J. Le Guen, N. Tucker, and K. Parker, "Thermo-mechanical, morphological and water absorption properties of thermoplastic starch/cellulose composite foams reinforced with PLA," *Cellulose*, vol. 26, pp. 4463–4478, 2019.

Supporting Information

Table S1: Summary of ANOVA and fitted regression model for respected responses after eliminating the non-significant model terms

Source		Apparent Density, g/cc (R_1)	Compressive Modulus, MPa (R_2)	Average Cell Size, µm (R_3)	Cell Density, × 10^5 cells/cc (R_4)
		p-value	*p*-value	*p*-value	*p*-value
Model	Value	0.0389	0.0465	0.0367	0.0493
	Observation	significant	significant	significant	significant
Main effects	Temperature, °C (A)	0.3597	0.4362	0.1993	0.0412
	Pressure, bar (B)	0.0710	0.3621	0.5627	0.046
	Time, h (C)	-*	0.0285	0.2502	0.284
Main effect interactions	*AB*	-*	0.1483	0.0147	0.0283
	AC	0.0143	0.0136	0.0055	0.163
	BC	-*	0.669	0.4111	0.2357
Second order interactions	A^2	0.2615	0.0433	-*	-*
	B^2	-*	-*	0.2244	0.4246
	C^2	0.1121	0.2122	0.2998	-*
R	R-square	0.6455	0.8144	0.8283	0.7549
	Adequate precision	6.4606	6.0274	8.2412	7.1574
Residual	Lack of fit (F-test)	0.0700	0.1956	0.095	0.0658
	Observation	not significant	not significant	not significant	not significant
Regression model	Responses:	Final equations in terms of coded factors:			
	Apparent density, g/cc (R_1)	$R_1 = 0.1394 - 0.0106A + 0.0223B + 0.0389AC + 0.0189A^2 + 0.0276C^2$			
	Compressive Modulus, MPa (R_2)	$R_2 = 1.85 + 0.1492A + 0.1762B - 0.4971C + 0.3491AB + 0.7039AC + 0.0959BC + 0.6389A^2 + 0.3561C^2$			
	Average Cell Size, µm (R_3)	$R_3 = 17.90 + 1.39A - 0.5962B - 1.23C - 3.75AB - 4.62AC - 1.02BC + 1.88B^2 - 1.58C^2$			
	Cell Density, cells × cm^3 (R_4)	$R_4 = 64.51 - 28.89A - 28.05B - 13.65C + 37.75AB + 21.72AC + 18.12BC - 14.31B^2$			

Note: * These insignificant model terms (*C, AB, BC,* A^2, B^2, C^2) were removed to improve the precision of the model.

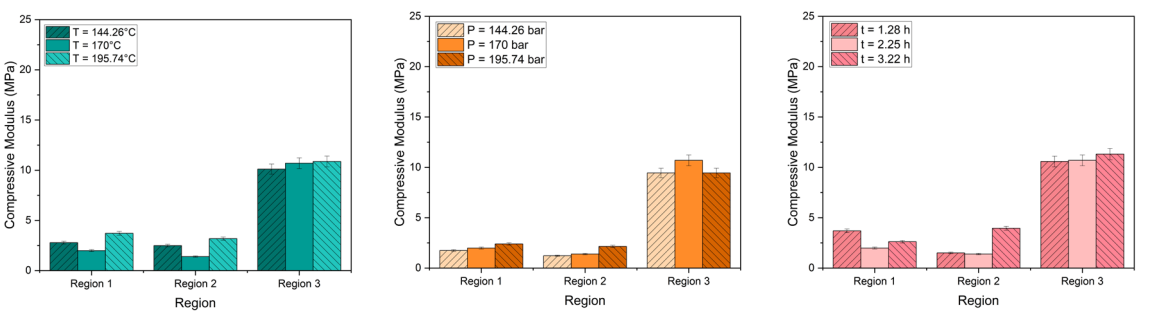

(a) (b) (c)

Figure S1: Compressive modulus of selected PLA foam samples at different regions: (a) variation of temperature, (b) variation of pressure, and (c) variation of time.

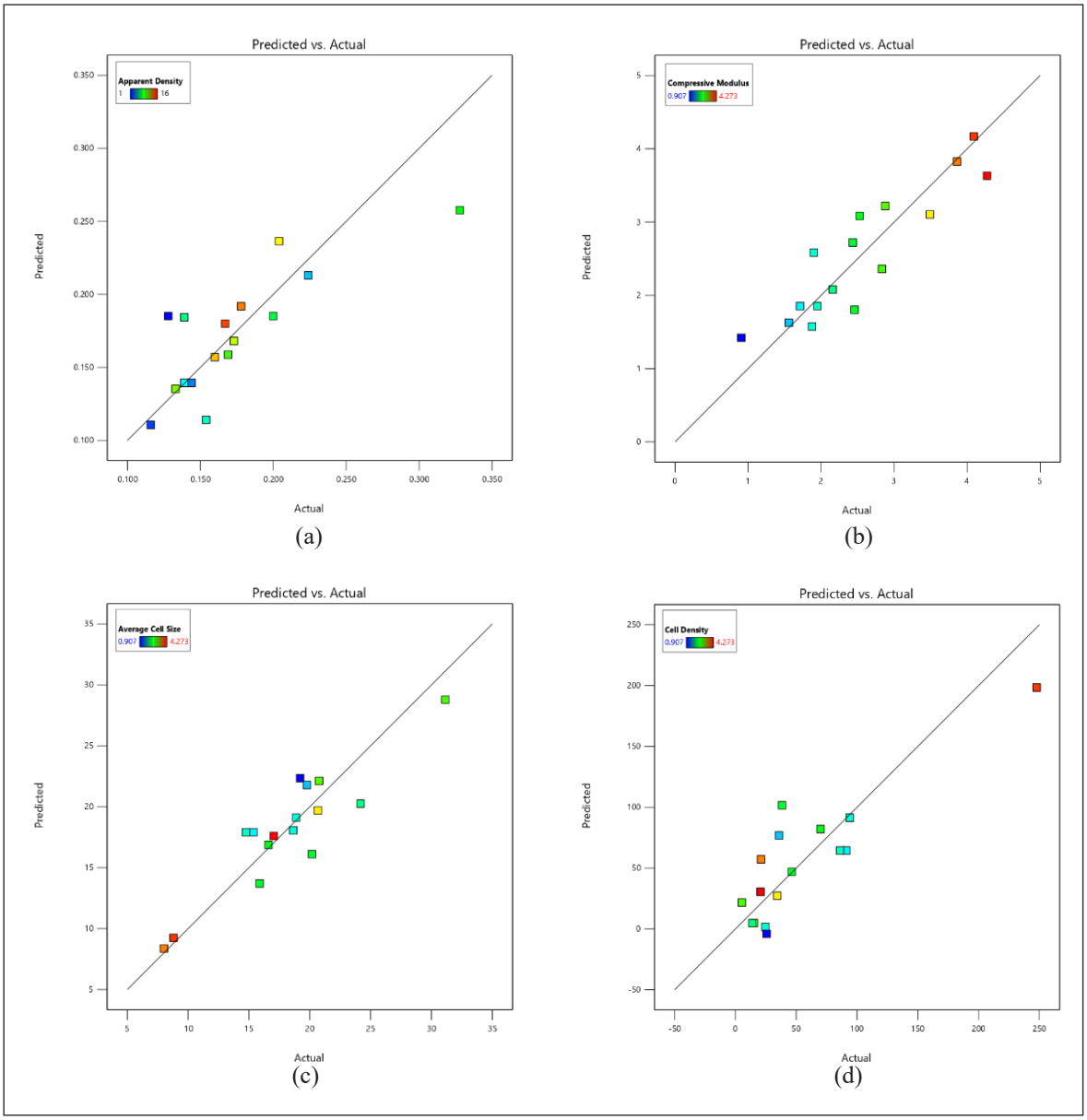

Figure S2: The correlation plots of predicted vs. actual values of the responses: (a) apparent density, (b) compressive modulus, (c) average cell size, and (d) cell density.

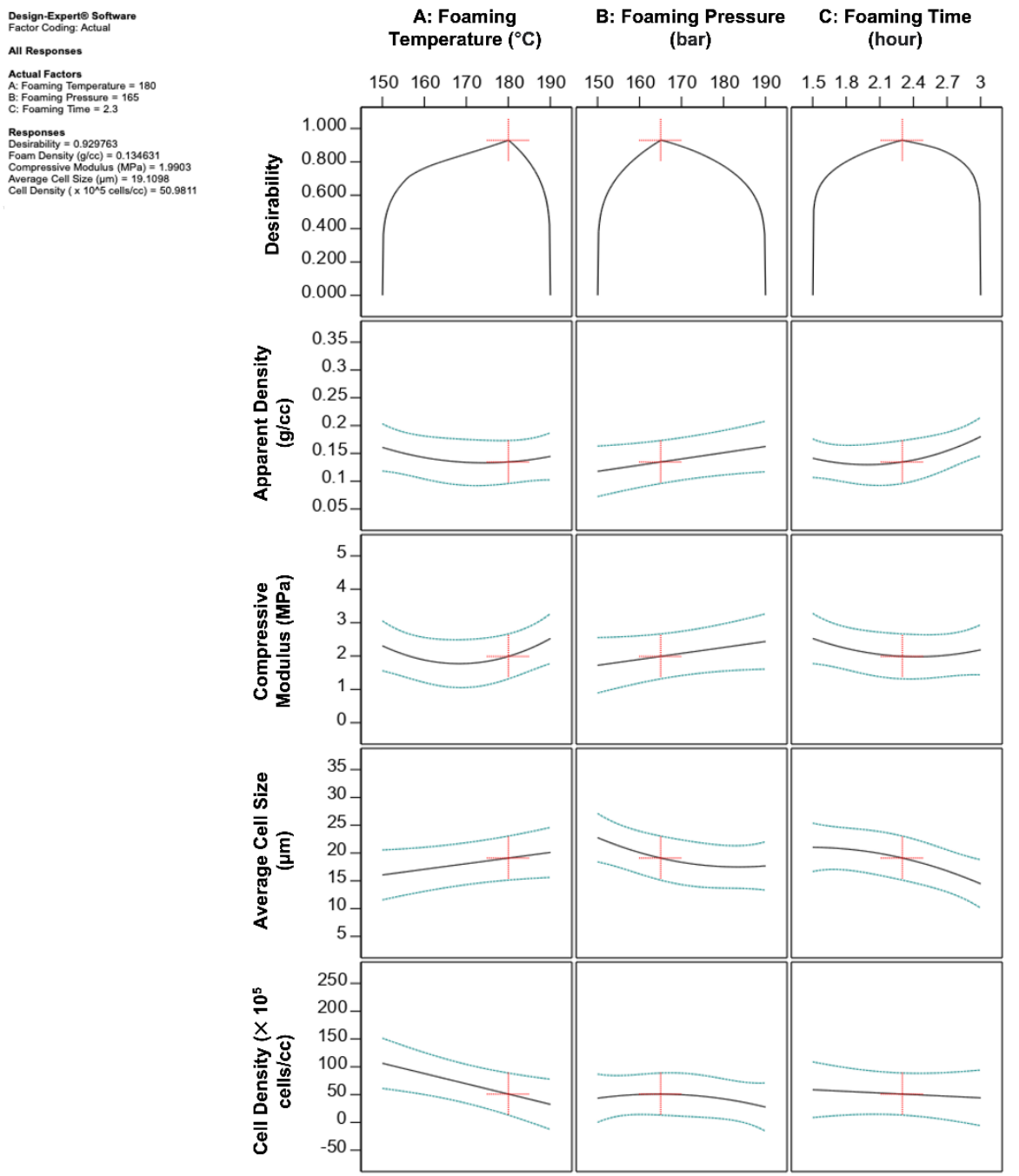

Figure S3: Optimal conditions for the foaming of PLA with their predicted values of responses and desirability score.

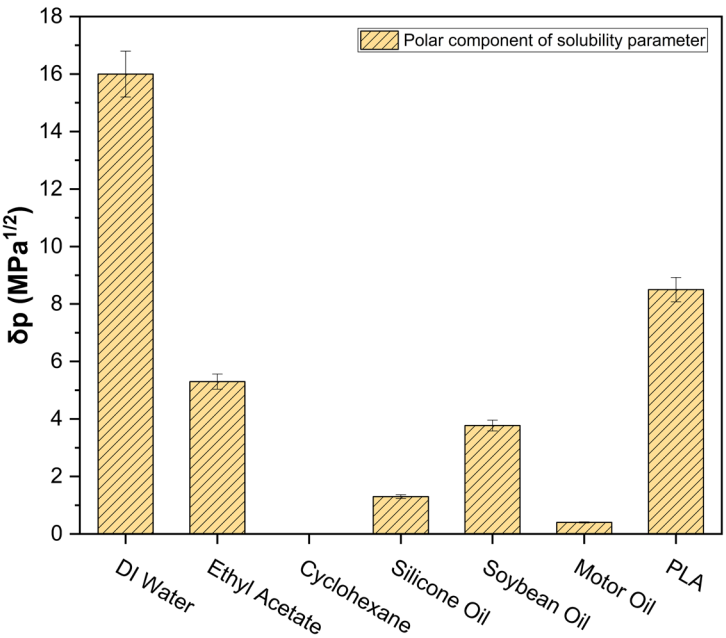

Figure S4: The solubility parameters of different test liquids and PLA [1]–[7].

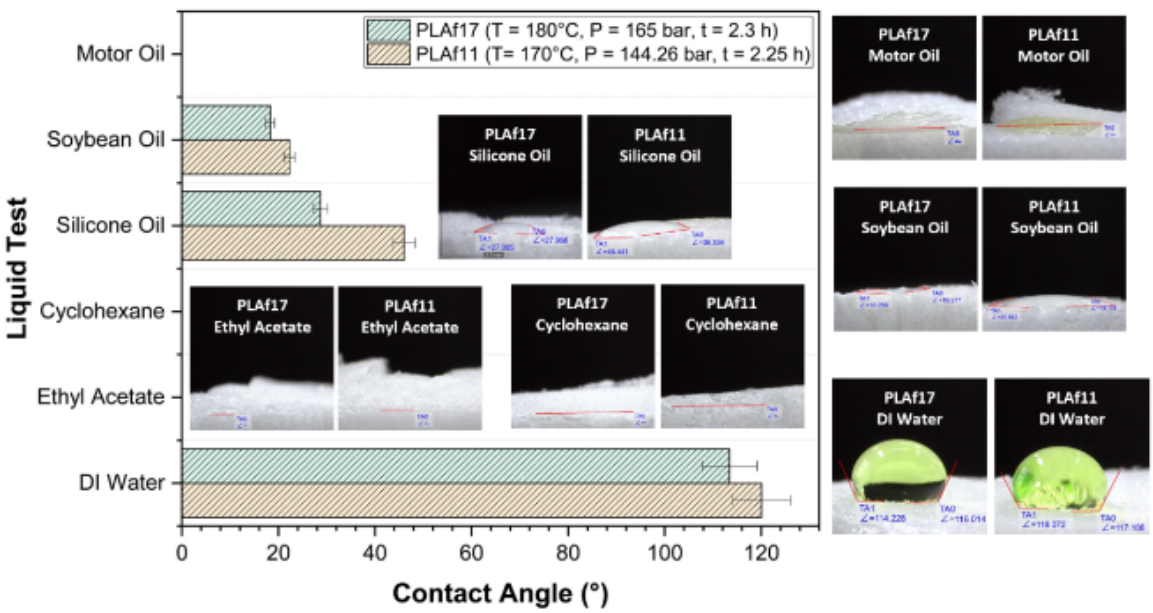

Figure S5: Average contact angle values of various liquids on the surface of selected PLA foam samples and their corresponding optical images.

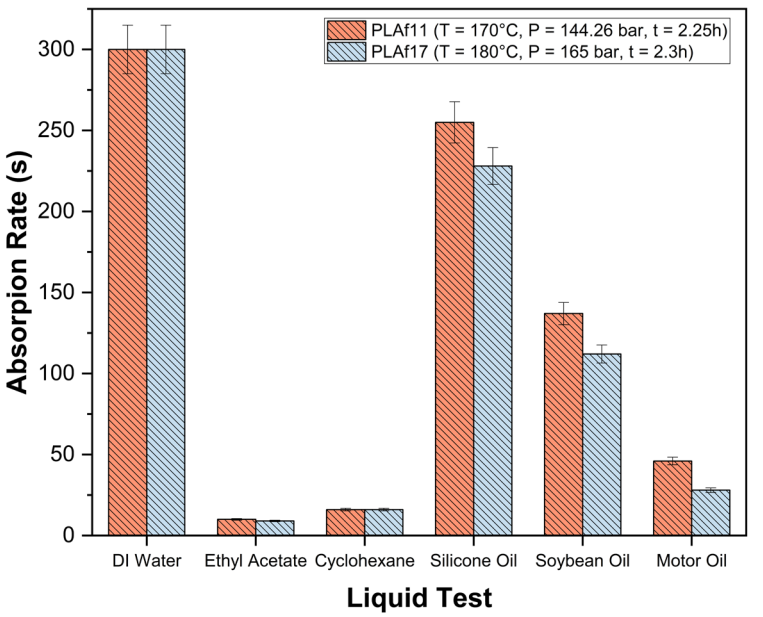

Figure S6: The absorption rates of various liquids to selected PLA foam samples.

References

[1] C. M. Hansen and A. Beerbower, "Solubility Parameters," *Encyclopedia of Chemical Technology*, vol. 2, pp. 889–910, 1971.

[2] A. F. Barton, *CRC Handbook of Solubility Parameters and other Cohesion Parameters*. London, UK: Routledge, 2017:

[3] A. Jarray, A. Feichtinger, and E. Scholten, "Linking intermolecular interactions and rheological behavior in capillary suspensions," *Journal of Colloid and Interface Science*, vol. 627, pp. 415–426, 2022.

[4] M. M. Batista, R. Guirardello, and M. A. Krähenbühl, "Determination of the Hansen solubility parameters of vegetable oils, biodiesel, diesel, and biodiesel–diesel blends," *Journal of the American Oil Chemists' Society*, vol. 92, no. 1, pp. 95–109, 2015.

[5] J. L. Gardon and J. P. Teas, "Characterization of Coatings: Physical Techniques," in *Treatise on Coatings*. New York: Marcel Dekker, 1976.

[6] A. Beerbower and J. Dickey, "Advanced methods for predicting elastomer/fluids interactions," *ASLE transactions*, vol. 12, no. 1, pp. 1–20, 1969.

[7] E. Meaurio, E. Sanchez-Rexach, E. Zuza, A. Lejardi, A. del Pilar Sanchez-Camargo, and J.-R. Sarasua, "Predicting miscibility in polymer blends using the Bagley plot: Blends with poly (ethylene oxide)," *Polymer*, vol. 113, pp. 295–309, 2017.